Breakdown of the Wiedemann-Franz law at the Lifshitz point of strained Sr_2RuO_4

Veronika C. Stangier,[1] Erez Berg,[2] and Jörg Schmalian[1,3]
[1]*Institute for Theory of Condensed Matter, Karlsruhe Institute of Technology, Karlsruhe 76131, Germany*
[2]*Department of Condensed Matter Physics, Weizmann Institute of Science, Rehovot, 76100, Israel*
[3]*Institute for Quantum Materials and Technologies, Karlsruhe Institute of Technology, Karlsruhe 76021, Germany*

(Received 6 August 2021; revised 11 February 2022; accepted 14 February 2022; published 9 March 2022)

Strain tuning Sr_2RuO_4 through the Lifshitz point, where the Van Hove singularity of the electronic spectrum crosses the Fermi energy, is expected to cause a change in the temperature dependence of the electrical resistivity from its Fermi liquid behavior $\rho \sim T^2$ to $\rho \sim T^2\log(1/T)$, a behavior consistent with experiments by Barber *et al.* [Phys. Rev. Lett. **120**, 076602 (2018)]. This expectation originates from the same multiband scattering processes with large momentum transfer that were recently shown to account for the linear in T resistivity of the strange metal $Sr_3Ru_2O_7$. In contrast, the thermal resistivity $\rho_Q \equiv T/\kappa$, where κ is the thermal conductivity, is governed by qualitatively distinct processes that involve a broad continuum of compressive modes, i.e., long-wavelength density excitations in Van Hove systems. While these compressive modes do not affect the charge current, they couple to thermal transport and yield $\rho_Q \propto T^{3/2}$. As a result, we predict that the Wiedemann-Franz law in strained Sr_2RuO_4 should be violated with a Lorenz ratio $L \propto T^{1/2}\log(1/T)$. We expect this effect to be observable in the temperature and strain regime where the anomalous charge transport was established.

DOI: 10.1103/PhysRevB.105.115113

I. INTRODUCTION

Sr_2RuO_4 is a fascinating material that combines electronic correlations and unconventional superconductivity whose mechanism has yet to be understood [1,2]. Major progress in our understanding of this material was achieved through the application of uniaxial stress. This leads to a more than twofold increase in the superconducting transition temperature [3] to $T_c^{\max} \approx 3.5\,\mathrm{K}$, a rich phase diagram [4,5], and puzzling behavior of thermodynamic properties with regards to time-reversal symmetry breaking [6]. The maximum in the superconducting transition temperature occurs for strain values $\varepsilon_{xx}^* \approx 0.45$. This is at or very near the Lifshitz transition [7] where a Van Hove singularity of the electronic spectrum crosses the Fermi energy [5].

Evidence that the normal state of the system is equally affected by this Lifshitz point was given by Barber *et. al* [8] in measurements of the electrical resistivity as function of strain ε_{xx} and is evident from recent measurements of the elasto-caloric effect [5]. The main finding of the transport measurements are as follows: For strain values below and above ε_{xx}^*, the resistivity shows Fermi liquid behavior with $\rho \approx \rho_0 + AT^2$, while for $\varepsilon_{xx} \approx \varepsilon_{xx}^*$ the resistivity is more singular. The data between T_c and about 40 K are consistent with $\rho = \rho_0 + AT^2\log(T_0/T)$. Over most of this temperature regime, the residual resistivity ρ_0 is a small fraction of the total resistivity. Hence, the system can be safely analyzed in the clean limit. Similar results were obtained by tuning the system to the Van Hove singularity by La^{3+} substituted $Sr_{2-y}La_yRuO_4$ [9,10] or epitaxial strain [11], however with somewhat larger values for the residual resistivity ρ_0.

In this paper we determine the electrical and thermal transport behavior due to electron-electron scattering of clean Sr_2RuO_4 near the strain-induced Lifshitz point. Distinct scattering processes, both impacted by the presence of a Van Hove singularity at the Fermi energy, affect charge and heat transport differently, leading to a violation of the Wiedemann-Franz law [12]. Charge transport is determined by large momentum transfer scattering that couples non-Van Hove to Van Hove states. Heat transport is dominated by long-wavelength scattering due to compressive modes that build a broad continuum due to the saddle point in the energy dispersion. For perfectly clean systems and ignoring the onset of superconductivity or other ordered states this behavior should continue down to lowest temperatures. The Wiedemann-Franz law should only be recovered once impurity scattering becomes dominant. As the two scattering rates that govern electrical and thermal transport are both caused by electron-electron interactions and the presence of the Van Hove singularity, we expect that the violation of the Wiedemann-Franz law occurs in the same temperature regime $3.5\,\mathrm{K} \cdots 20 - 40\,\mathrm{K}$ where the deviation from the T^2 behavior in the resistivity was observed [8]. Our results call for thermal conductivity measurements under strain to verify the importance of electron-electron interactions of the quasi-two-dimensional sheet of the Fermi surface.

The existence of logarithmic corrections to the T^2 behavior near Van Hove singularities was discussed in the past with $\rho \sim T^2\log^2(1/T)$ in Ref. [13] and $\rho \sim T^2\log(1/T)$ in Ref. [14]. Including impurity scattering then changes the behavior to $\rho = \rho_0 + BT^{3/2}$, where the T-dependent term is, however, a small correction to the residual resistivity. A careful analysis of the transport processes in systems with

impurity scattering was recently performed in Ref. [15]. Interestingly, in this paper a drop in the Lorenz ratio near the Van Hove singularity was found. As we will demonstrate in detail below, $\rho \sim T^2 \log(1/T)$ does indeed follow for Sr_2RuO_4, if one goes beyond these previous investigations and includes interband scattering events.

The above results are somewhat surprising as usually a single, *hot* point on the Fermi surface does not influence the transport properties of a system. A prime example is the transport behavior near a density-wave instability where hot spots are Fermi surface points connected by the ordering vector of the density wave [13,16]. While the scattering rate at these isolated points on the Fermi surface is singular, the transport is dominated by generic, *cold* regions of the Fermi surface that short circuit the contribution from the hot spots and lead to Fermi liquid behavior with $\rho \sim T^2$ [13]. Only the inclusion of impurity scattering changes the behavior to $\rho = \rho_0 + AT^{d/2}$ [17,18]. However, in this case the T-dependent term is a small correction to the dominant residual resistivity ρ_0, in distinction to the experimental result of Ref. [8].

An interesting exception to the rule that hot spots are irrelevant for transport was recently presented in Ref. [19] to explain the linear in T resistivity of the strange metal $Sr_3Ru_2O_7$. It was shown that scattering processes $cc \leftrightarrow ch$, in which a cold electron (c) becomes hot (h) after colliding with another cold electron, exists everywhere on the Fermi surface, i.e., it cannot be short circuited. For $Sr_3Ru_2O_7$ the hot electrons are made up of an exceptionally sharp peak in the density of states that crosses the Fermi surface. The relevance of this scenario for Sr_2RuO_4 was already mentioned in Ref. [19]. Below we show that for the specific Fermi surface geometry of Sr_2RuO_4 the $cc \leftrightarrow ch$ processes do indeed yield the $\rho \sim T^2 \log(1/T)$ of Ref. [14]. One has to be careful however to include all bands that cross the Fermi surface, as mere umklapp processes of a single band do not provide the necessary phase space for $cc \leftrightarrow ch$ processes down to lowest temperatures. Hence, our analysis shows that the electrical resistivity of strained Sr_2RuO_4 can be understood in terms of the $cc \leftrightarrow ch$ approach of Ref. [19].

As we discuss in more detail in Sec. II, the presence of a Van Hove singularity gives rise to distinct enhanced scattering cross sections for large momentum and long-wavelength scattering processes. This presence of distinct scattering processes that do and do not contribute to the resistivity suggests to analyze different transport properties. After all, the Wiedemann-Franz law, according to which the Lorenz ratio

$$L = \frac{\kappa}{\sigma T} = \frac{\rho}{\rho_Q} \tag{1}$$

of the thermal conductivity $\kappa = T/\rho_Q$ and the electronic conductivity $\sigma = 1/\rho$ approaches $L_0 = \frac{\pi^2}{3}(\frac{k_B}{e})^2$, is caused by the same scattering processes contributing to thermal and charge transport [20]. This is certainly the case for disordered electrons [21,22]. In clean Fermi liquids, charge current relaxation requires umklapp scattering, while heat current relaxation transport does not. Hence, there is no reason to expect that $L \to L_0$. However, given that both scattering rates are proportional to T^2 with $\tau_{J,Q}^{-1} = A_{J,Q} T^2$ for charge (J) and heat (Q) transport processes, one still expects a constant Lorenz ratio $L(T \to 0) \to L_0 \frac{A_J}{A_Q}$.

We show that the thermal transport at the Lifshitz point is governed by a scattering rate $\tau_Q^{-1} \propto T^{3/2}$ caused by the continuum of density fluctuations, while the resistivity follows the discussed $\tau_J^{-1} \propto T^2 \log \frac{D}{T}$ with bandwidth D. As a result, we obtain for the Lorenz ratio

$$L \propto T^{1/2} \log \frac{D}{T}, \tag{2}$$

which vanishes as $T \to 0$. Hence, we expect a strong breakdown of the Wiedemann-Franz law at the Lifshitz point of strained Sr_2RuO_4. These results are valid right at the Lifshitz transition. As the chemical potential moves away from the Van Hove point one expects to recover the usual Fermi liquid behavior. Figure 1 shows an interpolation between the two cases with

$$\rho(T) \approx A_J T^2 \log \frac{D}{\sqrt{T^2 + T^{*2}}} \tag{3}$$

and

$$\rho_Q(T) \approx A_Q T^2 \left(\frac{D^2}{T^2 + T^{*2}} \right)^{1/4}, \tag{4}$$

where singular contributions are cut off by the temperature scale T^*. This scale is essentially the distance of the Van Hove point to the Fermi energy and is sketched in the right inset of Fig. 1 using realistic parameters for the electronic structure of Sr_2RuO_4; see Appendix B for details. The left inset shows the Lorenz number as function of temperature. Our prediction for the violation of the Wiedemann-Franz law is consistent with the numerical solution of the Boltzmann equation of Ref. [15], where a suppression in the Lorenz number for weakly disordered systems was seen near the Van Hove point. This result can easily be generalized to a system with two Van Hove points, e.g., Sr_2RuO_4 under c-axis compression, as long as inter-Van Hove scattering does not lead to a density wave instability.

It is of interest to contrast the behavior found here with the one of two-dimensional Fermi liquids without Van Hove singularity. Then the single-particle scattering rate is enhanced by a logarithmic term, compared to the usual T^2 behavior $\tau_{qp}^{-1} \sim T^2 \log(D/T)$. As this enhancement is due to small momentum transfer processes, it will not affect the resistivity [23], i.e., $\rho(T) \sim T^2$. However, the thermal conductivity does couple to forward scattering processes and acquires an additional logarithmic contribution $\rho_Q(T) \sim T^2 \log(D/T)$ [24]. Hence one also finds a violation of the Wiedemann-Franz law $L(T) \sim 1/\log(D/T)$. This violation, however, is much weaker than the one we predict at a Van Hove point and therefore harder to observe experimentally.

In what follows we briefly discuss the electronic structure of Sr_2RuO_4 within a three-band model. We then summarize the behavior of long-wavelength density fluctuations near a Van Hove point. Finally we present our results for the charge and heat transport. In the appendices we comment briefly on the relation to Matthiessen's rule, summarize the tight-binding parametrization of the band structure, determine the single-particle scattering rate, and present our results for the current relaxation rate $\tau_J^{-1}(\omega)$ in the regime $\tau_J^{-1}(\omega = 0) \ll \omega \ll D$.

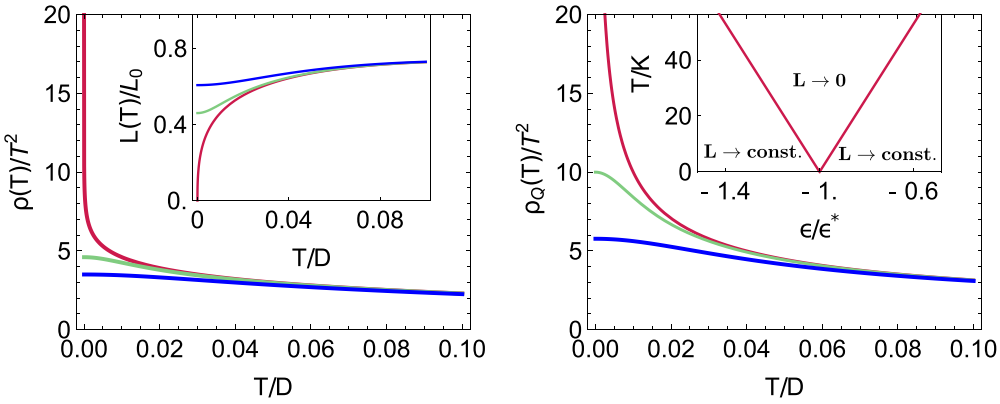

FIG. 1. Temperature dependence of the resistivity $\rho(T) \sim T^2 \log(D/T)$ (left) and thermal resistivity $\rho_Q(T) \sim T^{3/2}$ (right) divided by the Fermi liquid behavior T^2 at the Van Hove point (red curves). The more singular behavior of the thermal resistivity is clearly visible. D is the effective bandwidth of the problem. As one moves away from the Van Hove point, one expects a temperature scale T^* below which both transport coefficients recover ordinary Fermi liquid behavior following Eqs. (3) and (4). We use $T^*/D = 0.01$ (green curves) and $T^*/D = 0.03$ (blue curves). The inset shows the corresponding behavior for the Lorenz ratio $L(T)$. The right index shows the characteristic temperature scale T^* for the crossover to Van Hove dominated scattering as the strain is varied. We used the parameters given in Appendix B. In this inset we also indicate the regimes where the Lorenz number L tends to a finite value or vanishes as T decreases.

II. MODEL AND DENSITY RESPONSE

As we include multiband effects in our analysis we start from the following three-band model with kinetic energy

$$H_0 = \sum_{k\sigma} \psi^\dagger_{k\sigma} \mathcal{H}(\boldsymbol{k}) \psi_{k\sigma} \tag{5}$$

where $\psi_{k\sigma} = (d_{k,xy,\sigma}, d_{k,xz,\sigma}, d_{k,yz,\sigma})^T$ with annihilation operators for electrons in the Ru $4d_{xy}$ as well as $4d_{xz}$ and $4d_{yz}$ orbitals, respectively. For our analysis we use the single-particle Hamiltonian

$$\mathcal{H}(\boldsymbol{k}) = \begin{pmatrix} \varepsilon_{\boldsymbol{k}xy} & 0 & 0 \\ 0 & \varepsilon_{\boldsymbol{k}xz} & V_{\boldsymbol{k}} \\ 0 & V_{\boldsymbol{k}} & \varepsilon_{\boldsymbol{k}yz} \end{pmatrix}, \tag{6}$$

where we employ the dispersion relations obtained in Ref. [11] from angular-resolved photoemission data for the unstrained system. The d_{yz} and d_{xz} orbitals overlap and split into the α band located at the corners of the Brillouin zone and the β in the center. Both bands are moderately affected by a- or b-axis stress without qualitative changes in the dispersion. The γ band however, formed by the d_{xy} orbitals, is highly susceptible to strain and undergoes a Lifshitz transition under uniaxial pressure. We follow Ref. [8] to account for these changes in the dispersion at finite strain. Uniaxial strain ϵ_{xx} lifts the degeneracy between states at momenta $(\pi, 0)$ and $(0, \pi)$ and splits the Van Hove singularity into two peaks. For $\epsilon^*_{xx} = 0.45\%$ the Van Hove singularity at

$$\boldsymbol{k}_{\mathrm{VH}} = (0, \pi) \tag{7}$$

crosses the Fermi energy. The details of this analysis are summarized in Appendix B. In Fig. 2 we show our results for the strain dependence of the Fermi surface and the density of states.

The modifications of the electrical resistivity at the strain-tuned Lifshitz point are argued to be due to the divergent density of states at the Van Hove singularity with large momentum transfer in the involved scattering processes. Sr_2RuO_4 is of course a three-dimensional material. Hence, the logarithmic divergence in the density of states is cut off at some energy scale $t_\perp$ set by the interlayer hopping. However, this energy scale was shown in experiments to be only a few Kelvin [1]. This is consistent with the three-dimensional electronic structure where the dispersion in the c direction is particularly weak for in-plane momenta near the Van Hove point [25,26]. With $t_\perp$ comparable to T_c we will ignore these effects in what follows. In addition to these density of states effects, electrons near a Van Hove singularity are also expected to yield singular negative corrections to the compressibility or other elastic constants:

$$\delta C(T) \sim -\frac{D}{v_0} \log \frac{D}{T}, \tag{8}$$

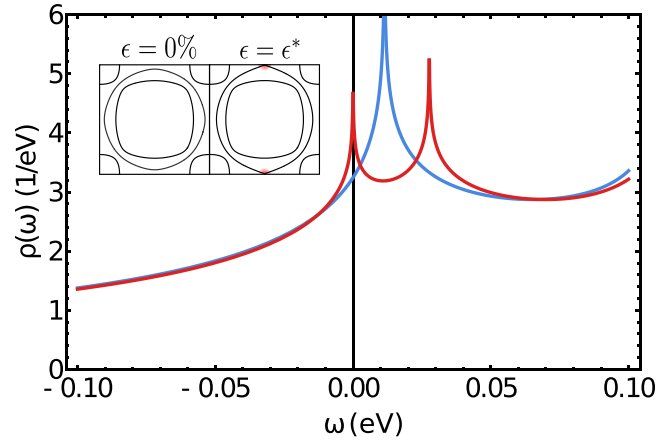

FIG. 2. Density of states of the γ band at zero strain (blue) and at the strain value ϵ^* that corresponds to the Lifshitz point where one of the strain-split Van Hove singularities crosses the Fermi energy (red). The inset shows the Fermi energies at zero strain (left) and at the Lifshitz point (right), where the hot parts of the Fermi surface are indicated in red.

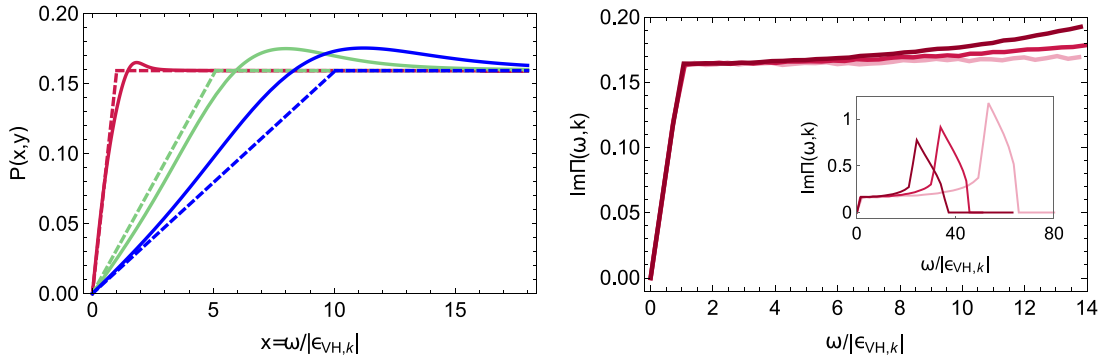

FIG. 3. Scaling function $P(x, y)$ (left) of Eq. (13) (solid lines) determining the frequency and temperature dependence of the charge excitation spectrum near a Van Hove point as function of $x = \omega/|\varepsilon_{\mathrm{VH},\boldsymbol{k}}|$, in comparison with the simplified version of Eq. (11) together with the substitution Eq. (14) (dashed lines) to include thermal effects. We used $m = 1$ and show results for $y = 0.1$ (red) $y = 5$ (green), and $y = 10$ (blue), where $y = T/|\varepsilon_{\mathrm{VH},\boldsymbol{k}}|$. The right panel shows the numerical result for the density excitation spectrum of the γ band at $T = 0$ for $q = 0.08\pi$ (dark red), $q = 0.06\pi$ (red), and $q = 0.04\pi$ (light red). For small $\omega/|\varepsilon_{\mathrm{VH},\boldsymbol{k}}|$ the curves show the expected scaling behavior. As shown in the inset, the result deviates from the approximated result for large $\omega/|\varepsilon_{\mathrm{VH},\boldsymbol{k}}|$.

where v_0 is the unit cell volume and D the band width. Unless preempted by other states of order, such as superconductivity, this should eventually give rise to a lattice instability at some low temperature. These compressive modes are related to a broad continuum in the long-wavelength density fluctuation spectrum of systems with Van Hove singularity [27]. Such fluctuations are known to give rise to singular single-particle scattering rates, with frequency and temperature dependencies that depend on the details of the band dispersion [27,28]. The corresponding contribution to the resistivity is small, however, since scattering of electrons from these fluctuations involves a small momentum transfer. The details of the electronic structure will be important when we analyze the kinematics of umklapp scattering events that are crucial for the electrical resistivity. In contrast, for the thermal transport long-wavelength density excitations of a system with Van Hove singularity will become important. The density excitation spectrum follows from

$$\mathrm{Im}\Pi(\boldsymbol{q},\omega) = \int \frac{d^2p}{4\pi}(f(\varepsilon_{\boldsymbol{p}+\boldsymbol{q}}) - f(\varepsilon_{\boldsymbol{p}})) \times \delta(\omega - \varepsilon_{\boldsymbol{p}+\boldsymbol{q}} + \varepsilon_{\boldsymbol{p}}) \tag{9}$$

where $f(\varepsilon)$ is the Fermi distribution function. As the low-momentum regime is dominated by states near the saddle point of the dispersion, we approximate the so called γ band with dispersion $\varepsilon_{\boldsymbol{k}xy}$ by

$$\varepsilon_{\boldsymbol{k}_{\mathrm{VH}}+\boldsymbol{p},xy} \approx \varepsilon_{\mathrm{VH},\boldsymbol{p}} = \frac{p_x^2 - p_y^2}{2m}. \tag{10}$$

At $T = 0$ the momentum integration can be performed easily, yielding [27]

$$\mathrm{Im}\Pi(\boldsymbol{q},\omega) = -\frac{m}{2\pi}\begin{cases} \frac{\omega}{|\varepsilon_{\mathrm{VH},\boldsymbol{q}}|} & \text{if} \quad |\omega| < |\varepsilon_{\mathrm{VH},\boldsymbol{q}}| \\ \mathrm{sign}(\omega) & \text{if} \quad |\omega| > |\varepsilon_{\mathrm{VH},\boldsymbol{q}}| \end{cases}. \tag{11}$$

This result is valid for $\omega < v_F|\boldsymbol{q}|$, where v_F is the maximum Fermi velocity away from the Van Hove point. The density excitation spectrum vanishes for $\omega \gg v_F|\boldsymbol{q}|$. This can be seen by imposing a momentum cutoff of the order of the Fermi momentum on the integration in Eq. (9). Comparing Eq. (11) to the usual density response of a Fermi gas, in the Van Hove case there is much more spectral weight at low frequencies.

At finite temperatures,

$$\mathrm{Im}\Pi(\boldsymbol{q},\omega) = P\left(\frac{\omega}{|\varepsilon_{\mathrm{VH},\boldsymbol{q}}|}, \frac{T}{|\varepsilon_{\mathrm{VH},\boldsymbol{q}}|}\right), \tag{12}$$

with scaling function

$$P(x,y) = \sqrt{y}\frac{m}{4\sqrt{\pi}}\left(Li_{1/2}\left(-e^{\frac{1}{4y}(2x-1)^2+\frac{2x}{y}}\right) - Li_{1/2}\left(-e^{\frac{1}{4y}(2x-1)^2}\right)\right) \tag{13}$$

and polylogarithmic function $Li_s(z)$. As we show in Fig. 3, the finite-temperature density response can be expressed to a good approximation in the form Eq. (11) but with

$$|\varepsilon_{\mathrm{VH},\boldsymbol{q}}| \to \Omega_{\boldsymbol{q}}(T) = \sqrt{\varepsilon_{\mathrm{VH},\boldsymbol{q}}^2 + T^2}. \tag{14}$$

The corresponding real part of the density response yields $\Pi(\boldsymbol{q}, 0) = -\frac{m}{\pi^2}\log\frac{D}{\Omega_{\boldsymbol{q}}(T)}$, which leads to Eq. (8) for the compressibility.

An important result that follows from this continuum of density excitations is an anomalous single-particle scattering rate [27,28]. To see this we analyze the imaginary part of the single-particle self-energy coupled to the above density fluctuations:

$$\mathrm{Im}\Sigma(\boldsymbol{k},\omega) = 2\frac{U^2}{N}\sum_{\boldsymbol{k}'}(f_0(\varepsilon(\boldsymbol{k}')) + n_0(\varepsilon(\boldsymbol{k}') - \omega)) \times \mathrm{Im}\Pi(\boldsymbol{k}-\boldsymbol{k}', \omega - \varepsilon(\boldsymbol{k}')), \tag{15}$$

where U is the electron-electron interaction and f_0 and n_0 are the Fermi and Bose distribution functions, respectively. While the momentum transfer $\boldsymbol{k} - \boldsymbol{k}'$ is small, the individual Fermi momenta $\boldsymbol{k}$ and $\boldsymbol{k}'$ do not necessarily have to be located in the vicinity of the Van Hove point. Indeed, the result $\mathrm{Im}\Sigma(\boldsymbol{k},\omega) \propto |\omega|^{\nu}$ for the single-particle self-energy depends sensitively whether $\boldsymbol{k}$ and $\boldsymbol{k}'$ are near or away from the saddle point of the dispersion. In the former case the dispersion $\varepsilon(\boldsymbol{k})$ is given by Eq. (10). In this case follows $\nu = 1$, which is the result obtained in Ref. [28]. Alternatively we can analyze

the self-energy for generic momenta. Now it is sufficient to assume a parabolic spectrum for $\varepsilon(\boldsymbol{k})$, which yields $\nu = 3/2$ [27]. A third option for momenta with parabolic dispersion and Fermi velocity parallel to the directions of zeros of Eq. (10) yields a somewhat more singular behavior with $\nu = 4/3$. We will show that the behavior with $\nu = 3/2$ is the one that determines the thermal conductivity. Further details of the analysis of the single-particle self-energy are summarized in Appendix D.

The nonanalytic result for the single-particle self-energy is non-Fermi liquid like. Nevertheless a quasiparticle description of the transport behavior seems justified. Indeed, a Kramers-Kronig transformation of this result yields that the quasiparticle weight $Z_{\mathbf{k}_F} = (1 - \frac{\partial \mathrm{Re}\Sigma_{\mathbf{k}_F}(\omega)}{\partial\omega})|_{\omega=0}$ remains finite.

III. ELECTRICAL RESISTIVITY

To calculate the resistivity we use the standard Boltzmann ansatz

$$\frac{\partial f_{\boldsymbol{k},i}}{\partial t} + e\boldsymbol{E}\cdot\frac{\partial f_{\boldsymbol{k},i}}{\partial \boldsymbol{k}} = -\mathcal{C}_{\boldsymbol{k},i}[f] \tag{16}$$

with band index $i \in \{\alpha, \beta, \gamma\}$ and scattering operator $\mathcal{C}_{\boldsymbol{k},i}[f]$, and determine the charge current

$$\boldsymbol{j} = -\frac{e}{N}\sum_{\boldsymbol{k},i,\sigma} \boldsymbol{v}_{\boldsymbol{k},i} f_{\boldsymbol{k},i} \tag{17}$$

at given electrical field. Next we expand $f_{\boldsymbol{k},i}$ for small deviations from equilibrium, parametrized by a function $\psi_{\boldsymbol{k},i}$ (proportional to the electric field $\boldsymbol{E}$):

$$f_{\boldsymbol{k},i} = f_0(\varepsilon_{\boldsymbol{k},i}) - T\frac{\partial f_0(\varepsilon_{\boldsymbol{k},i})}{\partial \varepsilon_{\boldsymbol{k}}}\psi_{\boldsymbol{k},i}. \tag{18}$$

The linearized collision operator due to electron-electron scattering up to second order in U takes the usual form

$$\begin{aligned}\mathcal{C}_{\boldsymbol{k},i}[\psi] = \frac{2\pi}{\hbar}\sum_{jkl}|U_{ijkl}|^2 \sum_{\boldsymbol{k}_2,\boldsymbol{k}_3,\boldsymbol{k}_4} L_{\varepsilon_{\boldsymbol{k}_1,i},\varepsilon_{\boldsymbol{k}_2,j},\varepsilon_{\boldsymbol{k}_3,k},\varepsilon_{\boldsymbol{k}_4,l}} \\ \times \delta\left(\varepsilon_{\boldsymbol{k}_1,i} + \varepsilon_{\boldsymbol{k}_2,j} - \varepsilon_{\boldsymbol{k}_3,k} - \varepsilon_{\boldsymbol{k}_4,l}\right) \\ \times \sum_{\boldsymbol{G}} \delta_{\boldsymbol{k}_1+\boldsymbol{k}_2-\boldsymbol{k}_3-\boldsymbol{k}_4-\boldsymbol{G}} \\ \times \left(\psi_{\boldsymbol{k}_1,i} + \psi_{\boldsymbol{k}_2,j} - \psi_{\boldsymbol{k}_3,k} - \psi_{\boldsymbol{k}_4,l}\right).\end{aligned} \tag{19}$$

The sum over $\boldsymbol{G}$ goes over the entire reciprocal lattice. In practice only a few terms contribute since four vectors of the first Brillouin zone only reach a finite number of reciprocal lattice vectors. U_{ijkl} refers to the intra- and interband matrix elements of the interaction, which we assume roughly to be of same order of magnitude $\sim U$. Below, we will discuss in detail which bands are included in the analysis. The phase space restrictions of degenerate fermions are included through

$$L_{\varepsilon_1,\varepsilon_2,\varepsilon_3,\varepsilon_4} = f_0(-\varepsilon_1)f_0(-\varepsilon_2)f_0(\varepsilon_3)f_0(\varepsilon_4). \tag{20}$$

Obviously $\psi_{\boldsymbol{k},i} \propto$ const. is a zero mode of the collision operator due to charge conservation. Similarly, $\psi_{\boldsymbol{k},i} \propto \varepsilon_{\boldsymbol{k},i}$ is a zero mode due to energy conservation. However, $\psi_{\boldsymbol{k},i} \propto k_\alpha$ is not a zero mode as the momenta do not have to add up to zero. Umklapp scattering processes spoil momentum conservation and yield a finite resistivity.

When analyzing the resistivity we make the simplifying assumption that

$$\psi_{\boldsymbol{k},i} \approx \psi_0 e\boldsymbol{E}\cdot\boldsymbol{v}_{\boldsymbol{k},i} \tag{21}$$

is determined by the velocity $\boldsymbol{v}_{\boldsymbol{k},i} = \frac{\partial\varepsilon_{\boldsymbol{k},i}}{\partial\boldsymbol{k}}$. This assumption is only justified if a given scattering process is kinematically allowed everywhere on the Fermi surface. Otherwise the coefficient ψ_0 will depend strongly on the position on the Fermi surface, effects that occur as corrections of the current vertex in a diagrammatic treatment of transport. As a result the longest scattering rate that is allowed on the entire Fermi surface dominates the transport behavior; it short circuits stronger scattering events that are kinematically only allowed on a subset of the Fermi surface. While this *hot spot* reasoning is well established [13,14,16–19], it appears at odds with the expectation based on Matthiessen's rule [29] where one has to add scattering rates, not times; see Appendix A. With the ansatz Eq. (21) we finally arrive at the following result for the low-frequency ($\omega < \tau_J^{-1}$) conductivity:

$$\sigma_{\alpha\beta}(\omega) = \frac{n_{D,\alpha\beta}}{-i\omega + \tau_J^{-1}}, \tag{22}$$

with Drude weight $n_{D,\alpha\beta} = \frac{e^2}{N}\sum_{\boldsymbol{k}\sigma}\frac{\partial^2\varepsilon_{\boldsymbol{k}}}{\partial k_\alpha \partial k_\beta} f_0(\varepsilon_{\boldsymbol{k}})$ and scattering rate for charge transport

$$\begin{aligned}\tau_J^{-1} = \frac{2\pi U^2 e^2}{\hbar}\sum_{ijkl}\sum_{\boldsymbol{k}_1,\boldsymbol{k}_2,\boldsymbol{k}_3,\boldsymbol{k}_4} L_{\varepsilon_{\boldsymbol{k}_1,i},\varepsilon_{\boldsymbol{k}_2,j},\varepsilon_{\boldsymbol{k}_3,k},\varepsilon_{\boldsymbol{k}_4,l}} \\ \times \delta\left(\varepsilon_{\boldsymbol{k}_1,i} + \varepsilon_{\boldsymbol{k}_2,j} - \varepsilon_{\boldsymbol{k}_3,k} - \varepsilon_{\boldsymbol{k}_4,l}\right) \\ \times \sum_{\boldsymbol{G}} \delta_{\boldsymbol{k}_1+\boldsymbol{k}_2-\boldsymbol{k}_3-\boldsymbol{k}_4-\boldsymbol{G}} \\ \times \left(v_{\boldsymbol{k}_1,i} + v_{\boldsymbol{k}_2,j} - v_{\boldsymbol{k}_3,k} - v_{\boldsymbol{k}_4,l}\right)^2.\end{aligned} \tag{23}$$

Due to the velocity term, momentum conserving scattering processes vanish in the single-band case and, as expected, do not contribute to the resistivity. For multiple bands momentum-conserving terms can, of course, change the current.

We perform the momentum summation according to

$$\frac{1}{N}\sum_{\boldsymbol{k}} F(\boldsymbol{k}) \approx \sum_S \int d\epsilon \rho_S(\epsilon)\int_S \frac{d\varphi}{2\pi} F(\epsilon,\varphi). \tag{24}$$

In the last step we sum over segments of the Fermi surface with essentially constant density of state $\rho_S(\epsilon) \approx \rho_F$ or with logarithmic density of state $\rho_S(\epsilon) \approx \rho_F \log(D/|\epsilon|)$. Finally we use

$$\begin{aligned}I = \int d\epsilon_1 \cdots d\epsilon_4 \delta(\epsilon_1 + \epsilon_2 - \epsilon_3 - \epsilon_4) L_{\epsilon_1,\epsilon_2,\epsilon_3,\epsilon_4} \\ \times \prod_{i=1}^{4}\rho_{S_i}(\epsilon_i) \approx \frac{2\pi^3}{3}T^3\rho_F^4 \log^n\frac{D}{T},\end{aligned} \tag{25}$$

where $n = 0\cdots 4$ is the number of electrons near a Van Hove point that are involved in a given scattering process. For example, for a $cc \to ch$ process, $n = 1$.

Depending on the number of such hot electrons involved, distinct scattering processes contribute differently to the resistivity. At first glance, the contribution of a scattering process with n hot electrons seems to be $\rho^{(n)} \propto T^2 \log^n(1/T)$, which would be dominated by $\rho^{(4)}$ at low T, i.e., by the largest value of n. However, as discussed above, we must (i) ensure the existence of umklapp scattering for given n, (ii) check that those processes exist on the entire Fermi surface, and (iii) ensure that some of the states involved have a finite velocity, needed to carry the current. We will see that this yields $n = 0$ for a single-band problem, while $n = 1$ if one includes additional bands that cross the Fermi energy. Hence, including multiband scattering events, the final result for the electrical resistivity will be

$$\rho(T) = A_J T^2 \log(D/T), \tag{26}$$

with $A_J \sim U^2 \rho_F^3 / n_D$. Equation (22) also includes the low-frequency Drude response of the system where τ_J corresponds to the zero-frequency limit of the charge transport rate. In Appendix E we also discuss $\tau_J^{-1}(\omega)$ in the opposite limit $\tau_J^{-1}(0) \ll \omega \ll D$ within a memory function approach and obtain

$$\tau_J^{-1}(\omega) \sim \omega^2 \log(D/|\omega|), \tag{27}$$

which determines the optical conductivity at these intermediate frequencies

$$\sigma_{\alpha\beta}(\omega) = \frac{n_{D,\alpha\beta}}{-i\omega(1+\lambda(\omega)) + \tau_J^{-1}(\omega)}. \tag{28}$$

Here, $\lambda(\omega) = \lambda_0(\log 2 - \frac{\omega}{D} \arctan(\frac{D}{\omega}))$ is the optical mass enhancement that follows from Kramers-Kronig transformation. This frequency dependency parallels the temperature dependency of the optical scattering rate at low frequencies.

For a problem with two Van Hove points at $\boldsymbol{k}_{\mathrm{VH}}^{(1)} = (\pi, 0)$ and $\boldsymbol{k}_{\mathrm{VH}}^{(2)} = (0, \pi)$, Eq. (26) was already obtained in Ref. [14]. Unlike in the former case, the full band structure, including the α and β sheets of the Fermi surface, need to be included to explain the anomalous resistivity down to lowest temperatures in Sr_2RuO_4. In what follows we discuss the kinematics of the single-band and multiband problems separately.

A. Resistivity for the γ band only

As we have seen, electron-electron scatterings yield different contributions to the resistivity, depending on the number of hot electrons involved. Which of these scattering processes are possible depends on the geometry of the Fermi surface. For simplicity, we start from a simplified model that includes only the γ band. In principle, the Fermi surface allows scattering processes with $n = 0$, 1, 2, and 4 hot electrons. Of these, only $cc \leftrightarrow cc$ (i.e., $n = 0$) and $cc \leftrightarrow ch$ ($n = 1$) contribute to the resistivity as they allow umklapp processes. Figure 4 shows the possible scatterings schematically for zero, one and two hot electrons.

The $cc \leftrightarrow ch$ scattering dominates the resistivity if every point on the cold Fermi surface can participate in such a scattering process. These processes have to be umklapp processes in order to contribute to the resistivity. It turns out that this is not possible for the entire Fermi surface. For an electron close to the Van Hove point the momentum transfer is not sufficiently large to surpass the gap between two neighboring Fermi surfaces. For the tight-binding parameters relevant for Sr_2RuO_4, we obtain that more than 10% of the Fermi surface cannot participate in $cc \leftrightarrow ch$ scattering processes. This implies that our assumption of Eq. (21) for the distribution function is not justified. Details on this calculations can be found in Appendix C.

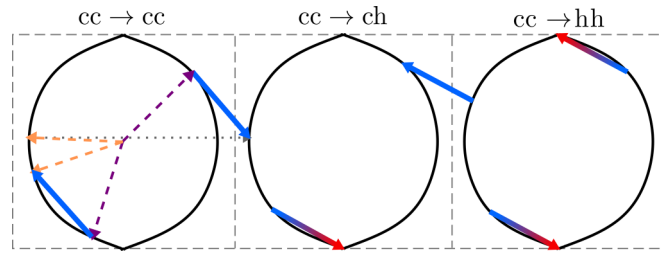

FIG. 4. A cc → cc process, where two electrons scatter from two cold initial states (purple) into two cold final states (orange) with umklapp scattering, leads to a resistivity of $\rho \propto T^2$. The solid arrows indicate the momentum transfer for each electron. An arrow starting at a cold momentum (blue end) can either end in another cold state (blue arrowhead) or in a Van Hove point (red arrowhead). The cc → ch process contributes by $\rho \propto T^2 \log(1/T)$ and dominates, if every point on the Fermi surface participates in this scattering. The cc → hh processes always conserve momentum, therefore they do not contribute to the resistivity.

States on the Fermi surface relatively close to the Van Hove point cannot participate in $cc \to ch$ umklapp scattering and should at sufficiently low temperatures lead to a resistivity that behaves as $\rho_{cc\to cc} \propto T^2$. One can qualitatively understand the crossover at higher temperature by considering two competing contributions to the resistivity with $\rho_{cc\to cc}$ and $\rho_{cc\to ch} \propto T^2 \log(1/T)$ that add up to the total resistivity

$$\rho_{ee}^{-1} \sim \rho_{cc\to cc}^{-1} + \rho_{cc\to ch}^{-1}. \tag{29}$$

At lowest T the resistivity exhibits the usual relation $\rho \propto T^2$, while at higher temperatures the $cc \to ch$ process dominates and the resistivity obtains the logarithmic correction $\rho \propto T^2 \log(1/T)$. The value of the crossover temperature can then be estimated as $T^* \sim D \exp(-c\frac{1-x}{x})$ where x is the fraction of the Fermi surface where cc ↔ ch scattering processes are kinematically forbidden and c is a numerical coefficient of order unity.

B. Resistivity with inter band scattering

So far we have restricted our analysis to the γ band. However, to explain the transport properties of Sr_2RuO_4, one has to take the whole Fermi surface into account. Since current is not conserved in interband scattering, no matter if it is umklapp or not, these scattering events contribute to the resistivity. Since the β band is convex and only includes cold regions (called c_β), we can always find a $c_\beta \to c_\beta$ process, as long as the momentum transfer is not too large. These processes fill the kinematic gap of the single-band case such that now the entire γ band can participate in $c_\beta c_\gamma \to c_\beta h_\gamma$ scattering, either by umklapp or interband scattering, as shown in Fig. 5. A similar argumentation can be made for the α band. Hence, additional *cold* states on the Fermi surface that can couple via interband

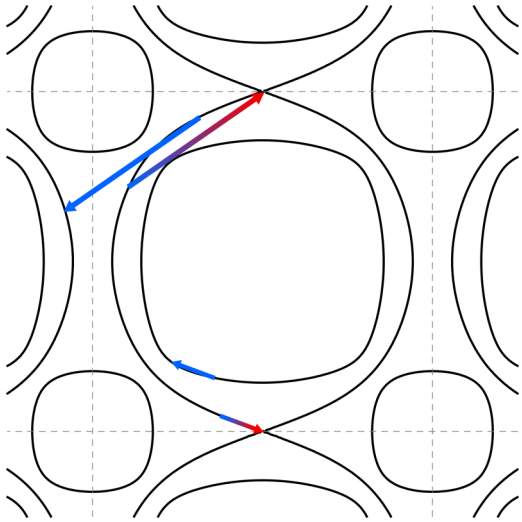

FIG. 5. When all bands are considered, every point on the cold Fermi surface can participate in cc → ch scattering, either by umklapp or inter band scattering.

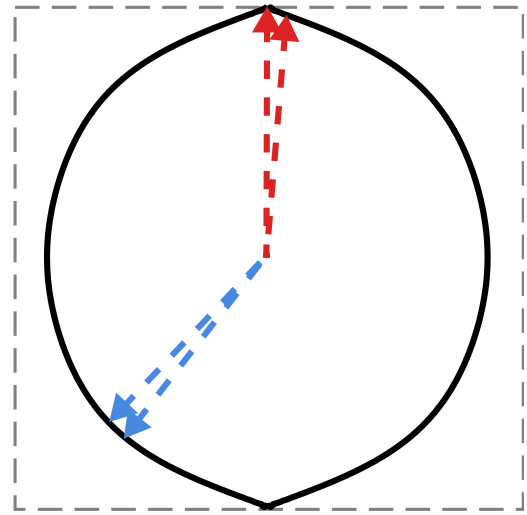

FIG. 6. ch → ch process dominating the thermal transport with two hot momenta near the Van Hove point (red) and two cold electrons with generic dispersion (blue). For small momentum transfer, this process is allowed everywhere on the Fermi surface.

collisions open up the phase space for singular scattering processes. This yields the somewhat surprising result that more cold states suppress the ability of these states to short circuit the singular transport processes that involve Van Hove points. Since all points on the α and β band can participate in $cc \leftrightarrow ch$ scattering processes and no new forbidden areas emerge, the resistivity follows Eq. (26) down to lowest temperatures.

IV. THERMAL TRANSPORT

Next, we analyze the thermal transport for a system at the Lifshitz point. For the thermal transport we start again from the Boltzmann equation

$$\frac{\partial f_{\boldsymbol{k},i}}{\partial t} + e\boldsymbol{v}_{\boldsymbol{k},i} \cdot \frac{\partial f_{\boldsymbol{k},i}}{\partial \boldsymbol{r}} = -\mathcal{C}_{\boldsymbol{k},i}[f] \tag{30}$$

with the same collision operator given in Eq. (19) for the electrical resistivity. The heat current

$$\boldsymbol{j}_Q = \frac{1}{N}\sum_{\boldsymbol{k},i,\sigma} (\varepsilon_{\boldsymbol{k},i} - \mu)\boldsymbol{v}_{\boldsymbol{k},i} f_{\boldsymbol{k},i} \tag{31}$$

is then determined as function of the temperature gradient, which enters the Boltzmann equation through

$$\frac{\partial f_{\boldsymbol{k},i}}{\partial \boldsymbol{r}} \approx -\frac{\partial f_0(\varepsilon_{\boldsymbol{k},i})}{\partial \varepsilon_{\boldsymbol{k}}} \frac{(\varepsilon_{\boldsymbol{k},i} - \mu)}{T} \frac{\partial T}{\partial \boldsymbol{r}}. \tag{32}$$

The crucial difference is of course that the momentum and the thermal current do not couple, i.e., there is no need to analyze whether umklapp scattering processes exist [30–35]. Hence, small momentum transfer collisions, where $\boldsymbol{q} = \boldsymbol{k}_3 - \boldsymbol{k}_1 = \boldsymbol{k}_2 - \boldsymbol{k}_4$ is small, contribute to the thermal resistivity. Of course, the two incoming momenta $\boldsymbol{k}_1$ and $\boldsymbol{k}_2$ can be far from each other, an issue that will be crucial when we determine the correct temperature dependence of the thermal conductivity.

We hence ignore umklapp processes in the thermal transport and perform one momentum sum using momentum conservation for the reciprocal lattice vector $\boldsymbol{G} = \boldsymbol{0}$. This yields for time-independent thermal gradients, including band indices $i, j = \alpha, \beta, \gamma$,

$$\begin{aligned}\boldsymbol{v}_{\boldsymbol{k}_1,i} \cdot \frac{\partial f_{\boldsymbol{k}_1,i}}{\partial \boldsymbol{r}} = \frac{2\pi U^2}{\hbar} \sum_{jkl} \sum_{\boldsymbol{k}_2,\boldsymbol{q}} L_{\varepsilon_{\boldsymbol{k}_1,i},\varepsilon_{\boldsymbol{k}_2,j},\varepsilon_{\boldsymbol{k}_1+\boldsymbol{q},k},\varepsilon_{\boldsymbol{k}_2-\boldsymbol{q},l}} \\ \times \delta\left(\varepsilon_{\boldsymbol{k}_1,i} +, \varepsilon_{\boldsymbol{k}_2,j} - \varepsilon_{\boldsymbol{k}_1+\boldsymbol{q},k} - \varepsilon_{\boldsymbol{k}_2-\boldsymbol{q},l}\right) \\ \times \left(\psi_{\boldsymbol{k}_1,i} + \psi_{\boldsymbol{k}_2,j} - \psi_{\boldsymbol{k}_1+\boldsymbol{q},k} - \psi_{\boldsymbol{k}_2-\boldsymbol{q},l}\right).\end{aligned} \tag{33}$$

We consider a generic momentum $\boldsymbol{k}_1$ on the Fermi surface. For small momentum transfer $\boldsymbol{k}_1 + \boldsymbol{q}$ will then be near $\boldsymbol{k}_1$. For the other incoming momentum $\boldsymbol{k}_2$ we can, however, assume that it is located in the vicinity of the Van Hove point, which implies that $\boldsymbol{k}_2 - \boldsymbol{q}$ is also near that point; see Fig. 6. Following our analysis for the charge transport, one might be tempted to conclude that the resistivity has $n = 2$ states near the Van Hove point, which would imply a scattering rate that behaves as $T^2 \log^2(1/T)$. However, as we saw in the analysis of the density fluctuation spectrum in Eqs. (11)–(13), small momentum transfer processes have a much increased phase space, which gives rise to a more singular behavior for the thermal transport.

To proceed we first make the ansatz for the distribution function

$$\psi_{\boldsymbol{k},i} = \psi_0 \frac{\varepsilon_{\boldsymbol{k},i} - \mu}{T} \boldsymbol{v}_{\boldsymbol{k},i} \cdot \nabla T, \tag{34}$$

which is analog to Eq. (21) for thermal transport. As before, we have to demonstrate that a given scattering process is present everywhere on the Fermi surface in order to justify the assumption that the coefficient ψ_0 is weakly dependent on momentum. With Eq. (34) and given the vanishing velocity at the Van Hove point, we can safely neglect $\psi_{\boldsymbol{k}_{2,4}}$ in Eq. (33). If we use the identity $f_0(\varepsilon)f_0(-\varepsilon') = (f_0(\varepsilon) - f_0(\varepsilon'))n_0(\omega)$ for $\varepsilon' = \varepsilon + \omega$ we can express the sum over $\boldsymbol{k}_2$, which runs over states near the Van Hove point, in terms of the density

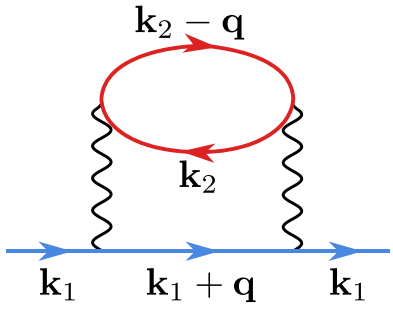

FIG. 7. Self-energy diagram determining the thermal resistivity with hot momenta $\mathbf{k}_2$ and $\mathbf{k}_2 - \mathbf{q}$ with hyperbolic dispersion (red) and cold momenta $\mathbf{k}_1$ and $\mathbf{k}_1 + \mathbf{q}$ with parabolic dispersion (blue).

spectrum of Eq. (9)

$$\boldsymbol{v}_{\boldsymbol{k}_1} \cdot \frac{\partial f_{\boldsymbol{k}_1}}{\partial \boldsymbol{r}} = -\frac{2\pi U^2 T}{\hbar N} \frac{\partial f_0(\varepsilon_{\boldsymbol{k}_1})}{\partial \varepsilon_{\boldsymbol{k}_1}} \sum_{\boldsymbol{q}} (\psi_{\boldsymbol{k}_1} - \psi_{\boldsymbol{k}_1 - \boldsymbol{q}}) \times (n_0(\varepsilon_{\boldsymbol{k}_1 - \boldsymbol{q}} - \varepsilon_{\boldsymbol{k}_1}) + f_0(\varepsilon_{\boldsymbol{k}_1 - \boldsymbol{q}})) \times \mathrm{Im}\Pi(\boldsymbol{q}, \varepsilon_{\boldsymbol{k}_1} - \varepsilon_{\boldsymbol{k}_1 - \boldsymbol{q}}). \tag{35}$$

Here we have for simplicity dropped the band indices. We will discuss the issue of interband processes below. In Eq. (35), we explicitly see how the coupling to compressive fluctuations affects the thermal conductivity. One now finds that, up to numerical factors of order unity, the collision operator is merely determined by the single-particle self-energy of Eq. (15):

$$\boldsymbol{v}_{\boldsymbol{k}_1} \cdot \frac{\partial f_{\boldsymbol{k}_1}}{\partial \boldsymbol{r}} = \tau^{-1}_{\boldsymbol{k}_1 Q} T \frac{\partial f_0(\varepsilon_{\boldsymbol{k}_1})}{\partial \varepsilon_{\boldsymbol{k}_1}} \psi_{\boldsymbol{k}_1} \tag{36}$$

with the heat transport scattering rate

$$\tau^{-1}_{\boldsymbol{k}_1 Q} \approx -2\mathrm{Im}\Sigma(\boldsymbol{k}_1, \varepsilon_{\boldsymbol{k}_1}). \tag{37}$$

This process is kinematically allowed everywhere on the Fermi surface, and amounts to an analysis of the self-energy diagram shown in Fig. 7. In Appendix D we summarize the analysis of the self-energy, see also Refs. [27,28]. While there exists more singular scattering in some parts of the Fermi surface, a generic point obeys

$$\tau^{-1}_{\boldsymbol{k},Q} = \frac{16U^2\rho_F^2}{3\sqrt{D}} T^{3/2}. \tag{38}$$

This yields for the thermal conductivity

$$\kappa = \frac{1}{TN} \sum_{\boldsymbol{k}\sigma} v_{\boldsymbol{k}}^2 \tau_{\boldsymbol{k},Q} \left(-\frac{\partial f_0(\varepsilon_{\boldsymbol{k}})}{\partial \varepsilon_{\boldsymbol{k}}} \right) (\varepsilon_{\boldsymbol{k}} - \mu)^2. \tag{39}$$

Performing the integrals in the usual manner yields for the thermal resistivity introduced in Eq. (1) the result

$$\rho_Q = A_Q D^{1/2} T^{3/2}, \tag{40}$$

where the coefficient A_Q is of the same order of magnitude as A_J that determines the charge transport in Eq. (26). The momentum transfer that gives rise to the anomalous power laws is small. However, we considered one initial state near the Van Hove singularity and another one at a generic momentum anywhere on the Fermi surface, not even on the same Fermi surface sheet. While both momenta change by small amounts they can be far apart in the Brillouin zone. Hence we include interband scattering. Had we restricted our analysis to intraband scattering processes with all momenta near the Van Hove singularity, a different, more singular power law would have emerged, with $\rho_Q \propto T$,. Thus processes that include the entire Fermi surface are included in our theory. The anomalous power law for the thermal conductivity is therefore independent on the details of the shape of the Fermi surface, provided it includes the Van Hove point.

This finally yields the Lorenz number

$$L = \frac{A_J}{A_Q D^{1/2}} T^{1/2} \log\left(\frac{D}{T}\right) \tag{41}$$

and the concomitant violation of the Wiedemann-Franz law.

V. CONCLUSIONS

In conclusion, we analyzed the electrical and thermal transport of clean Sr_2RuO_4 under strain near the Lifshitz point where a Van Hove singularity of the γ sheet of the Fermi surface crosses the Fermi energy. Based on the observation of well defined quasiparticles in this material we perform a quasiclassical Boltzmann transport theory. For larger frequencies, we also present results for the optical conductivity within a memory function approach. We find that both the electrical and the thermal transport are affected by the vicinity to the Lifshitz point. The known result for the electrical resistivity, discussed already in Ref. [14], is physically interpreted in terms of scattering processes where an electron near the Van Hove point collides with a *cold* electron away from the Van Hove point and scatters into two other cold states. This gives rise to a logarithmic enhancement of the charge transport rate $\tau_J^{-1} \sim T^2 \log(1/T)$ and hence of the electrical resistivity, consistent with observations of Refs. [8–11]. In particular, the observation by Barber *et al.* [8], with a very small residual resistivity ρ_0, demonstrate that an understanding of these results has to be achieved without resorting to impurity scattering processes that usually increase the phase space for singular electron-electron scattering [17]. For the specific electronic structure of Sr_2RuO_4 we show that the logarithmic enhancement is present down to lowest temperatures if one includes interband scattering processes. The reason is that intraband scattering requires umklapp processes, which have more stringent phase space requirements. Hence, the anomalous transport behavior seen in Sr_2RuO_4 is particularly robust as there are several bands that cross the Fermi surface. The situation is drastically different if one analyses thermal transport. Systems with Van Hove singularities are characterized by a much enhanced phase space of long-wavelength compressive modes. These compressive modes do not couple to charge transport. However, they are able to relax the thermal current and give rise to a thermal transport rate $\tau_Q^{-1} \propto T^{3/2}$. This result is valid in both the single- and multiband models, as it is independent of the exact geometry of the Fermi surface. As a consequence the Wiedemann-Franz law is violated with a Lorenz number that vanishes with a power law plus logarithmic corrections. The experimental confirmation of this prediction would in particular demonstrate the importance of the mentioned compressive modes for the low-energy excitations of Sr_2RuO_4. This would also be of interest as it would be curious to study whether these long-wavelength modes might

enhance an existing or even cause an instability towards a superconducting state. A related issue is clearly the role of higher-order processes not included in our analysis. The fact that the compressibility is guaranteed to vanish at a finite temperature is clear evidence that the system will eventually undergo some kind of instability. Our transport theory is however expected to be valid in the regime that leads up to this instability. Finally, given the presence of $5d$ elements, we should comment on the role of the spin-orbit coupling. Given the inversion symmetry of the material, the electronic states continue to be characterized by a Kramers pseudo-spin label. In this sense is the inclusion of spin-orbit coupling in our formalism rather straightforward. In fact, we do not expect our results to be affected in a qualitative manner by spin orbit effects. In addition, the weak dispersion along the c direction, essential for the importance of effectively two-dimensional Van Hove physics, was shown to be a consequence of by spin-orbit effects [25].

Our prediction for a violation of the Wiedemann-Franz law is only valid as long as one is in the clean regime. At some low temperature, impurity scattering effects should become important. Then we expect to recover at lowest temperatures the Wiedemann-Franz law where L approaches $L_0 = \frac{\pi^2}{3}(k_B/e)^2$, even at the Van Hove point. For the leading low-temperature corrections, still dominated by impurity scattering events, one expects $\tau_{Q,J}^{-1} = \tau_{\rm imp}^{-1} + C_{Q,J}T^{3/2}$, i.e., both transport rates should follow the same temperature dependence. Here the constant C_Q enters the rate for heat transport and C_J for the charge transport, respectively. The result for the temperature-dependent corrections of the charge scattering rate was obtained in Ref. [14]. An analogous reasoning yields the corresponding result for the heat transport. Most importantly, the leading terms are the impurity contributions and those should be the same, even if one includes phenomena such as weak localization corrections; see Ref. [21]. The transition between the regimes with and without Wiedemann-Franz law occurs when the charge scattering rate for clean systems becomes comparable to the impurity scattering rate. The temperature dependencies of scattering rates with impurities and the crossover behavior between different regimes could be relevant for the observations of La-substituted systems [10,11]. Again, its confirmation would give strong evidence for the importance of compressive modes for the low-energy electronic degrees of freedom.

ACKNOWLEDGMENTS

We are grateful to M. Garst, S. A. Hartnoll, C. Hicks, and A. P. Mackenzie for useful discussions. V.C.S. and J.S. were supported by the Deutsche Forschungsgemeinschaft (DFG, German Research Foundation) - TRR 288-422213477 Elasto-Q-Mat (Project No. B01). E.B. was supported by the European Research Council (ERC) under Grant HQMAT (Grant Agreement No. 817799), the Minerva foundation, and a Research Grant from Irving and Cherna Moskowitz.

APPENDIX A: MATTHIESEN'S RULE AND HOT VERSUS COLD CARRIERS

According to Matthiesen' s rule, the total resistivity is the sum of resistivities of different scattering mechanisms, $\rho_{\rm tot} = \rho_{\rm imp} + \rho_{\rm e-ph} + \rho_{\rm e-e}$, meaning that the dominant contribution to the resistivity comes from the shortest life time. This seems in sharp contrast to what was discussed in Eq. (29) and to our strategy to ensure that a given scattering mode is not short circuited by scattering processes on the Fermi surface with smaller rate. To clarify this issue we consider the linearized Boltzmann equation in the operator form

$$\hat{C}|\psi\rangle = |S\rangle, \tag{A1}$$

where $\hat{C}$ is the collision operator, $\psi_{\boldsymbol{k}} = \langle \boldsymbol{k} \mid \psi\rangle$ the correction to the distribution function and $S_{\boldsymbol{k}} = \langle \boldsymbol{k} \mid S\rangle$ some external source term. The source term due to an external electric field is $S_{\boldsymbol{k}} \equiv -\frac{e}{T}\boldsymbol{E}(\boldsymbol{q},\omega)\cdot \boldsymbol{v}_{\boldsymbol{k}}$. With the collision integral $\mathcal{C}_{\boldsymbol{k}}$ that we used in the main text, the operator is defined as

$$\hat{C}\psi_{\boldsymbol{k}} = \frac{1}{-T\frac{\partial f^{(0)}(\varepsilon_{\boldsymbol{k}})}{\partial \varepsilon_{\boldsymbol{k}}}}\int_{\boldsymbol{k}'}\frac{\delta \mathcal{C}_{\boldsymbol{k}}}{\delta \psi_{\boldsymbol{k}'}}\psi_{\boldsymbol{k}'}. \tag{A2}$$

It is a Hermitian operator with respect to the inner product

$$\langle \phi \mid \psi\rangle = \int_{\boldsymbol{k}} w_{\boldsymbol{k}}\phi_{\boldsymbol{k}}^*\psi_{\boldsymbol{k}} \tag{A3}$$

with weight function $w_{\boldsymbol{k}} = -T\frac{\partial f^{(0)}(\varepsilon_{\boldsymbol{k}})}{\partial \varepsilon_{\boldsymbol{k}}} > 0$. The entropy production can then we written as $\partial S/\partial t = \langle\psi|\hat{C}|\psi\rangle$, i.e., the operator is positive definite. The eigenvalues of the collision operator are the scattering rates

$$\hat{C} = \sum_{\lambda}|\lambda\rangle\tau_{\lambda}^{-1}\langle\lambda|, \tag{A4}$$

where λ labels distinct modes of the scattering process. For a rotation-invariant problem they could for example describe different angular momentum modes.

If the system is governed by several, distinct scattering mechanism, such as impurity, electron-phonon, or electron-electron scattering, the individual operators add up

$$\hat{C} = \hat{C}_{\rm imp} + \hat{C}_{\rm el-ph} + \hat{C}_{\rm el-el}.$$

We write this as $\tau_{\lambda}^{-1} = \sum_s \tau_{\lambda,s}^{-1}$ where the index s indicates the scattering mechanisms. In order to determine the distribution function we now have to invert the collision operator in the subspace orthogonal to zero modes that indicate conserved quantities such as particle number or energy. This is possible as long as these zero modes are orthogonal to the source term $|S\rangle$. It follows

$$\begin{aligned}|\psi\rangle &= \hat{C}^{-1}|S\rangle \\ &= {\sum_{\lambda}}'|\lambda\rangle\frac{1}{\sum_s \tau_{\lambda,s}^{-1}}\langle\lambda \mid S\rangle,\end{aligned} \tag{A5}$$

where the prime in the sum indicates that the inversion has been performed in the subspace orthogonal to the mentioned zero modes. In many instances, the scattering rates for nonzero modes depend weakly on the eigenmode index λ. Then one obtains the total scattering rate

$$\tau_{\rm tot}^{-1} = \sum_s \tau_s^{-1}. \tag{A6}$$

This leads to Matthiesen' s rule. However, if one considers a system with one dominant scattering mechanism, e.g., a clean

system with electron-electron scattering where phonons are frozen out at low temperatures, as we assume in this paper, then

$$|\psi\rangle = \sum_{\lambda} |\lambda\rangle \tau_{\lambda,\mathrm{el-el}} \langle \lambda \mid S\rangle. \tag{A7}$$

For systems where distinct eigenmodes of the scattering process under consideration vary strongly, as happens for strongly momentum dependent scattering rates, the largest scattering time dominates and we obtain a relation like given in Eq. (29).

To summarize, an electron that is exposed to different scattering mechanisms must cope with all of them and the rates add according to Matthiesen' s rule; different scattering mechanisms act like resistors in series. On the other hand, if there are different modes of one dominant mechanism, the longest scattering times dominate the conductivity; different modes act like resistors that are in parallel where the weakest scattering short circuits the transport.

APPENDIX B: TIGHT-BINDING PARAMETERS AND STRAIN DEPENDENCE OF THE ELECTRONIC STRUCTURE

We consider the electronic structure of Sr_2RuO_4 under arbitrary in-plane strain. The Van Hove singularity near the Fermi energy is due to the so called γ band, made of $4d_{xy}$ states. Its dispersion is given by the tight binding approximation

$$\begin{aligned}\varepsilon_{\boldsymbol{k},xy} = &-2t_{1,x}\cos k_x - 2t_{1,y}\cos k_y - \mu. \\ &-2(t_{4,+}\cos(k_x+k_y) + t_{4,-}\cos(k_x-k_y)).\end{aligned} \tag{B1}$$

with nearest and next-to-nearest-neighbor coupling parameters $t_{1,x/y}$ and $t_{4,+/-}$, respectively. It is natural to assume that for strained systems $t_{1,x}$ only depends on the change of the nearest neighbor distance a_x, $t_{1,y}$ only on a_y, while $t_{4,+}$ and $t_{4,-}$ are functions of the diagonal distance d_+ and counter-diagonal distance d_-, respectively. For simplicity we only consider in-plane strain ϵ_{ij}. The nearest-neighbor distances of the strained system are $a_i \approx a_0(1+\epsilon_{ii})$ and $d_\pm \approx \sqrt{2}a_0(1+\frac{1}{2}(\epsilon_{xx}+\epsilon_{yy}\pm 2\epsilon_{xy}))$. Following Ref. [8] it is reasonable to use $t_{1,i} = t_1(1-\alpha\epsilon_{ii})$ and $t_{4,\pm}/t_4 = 1-\frac{\alpha}{2}(\epsilon_{xx}+\epsilon_{yy}\pm 2\epsilon_{xy})$, where α is a tuning parameter. Assuming stress σ_{xx} along the x direction follows $\epsilon_{xy}=0$ and $\epsilon_{yy} = -\nu_{xy}\epsilon_{xx}$ with Poisson ratio ν_{xy} such that

$$\begin{aligned} t_{1,x} &= t_1(1-\alpha\epsilon_{xx}), \\ t_{1,y} &= t_1(1+\alpha\nu_{xy}\epsilon_{xx}), \\ t_{4,\pm} &= t_4\Big(1-\frac{\alpha}{2}(1-\nu_{xy})\epsilon_{xx}\Big). \end{aligned} \tag{B2}$$

Using the elastic constants of Ref. [36] yields $\nu_{xy}=0.39$. From Ref. [11] we take $t_1 = 0.119\,\mathrm{eV}$ and $t_4 = 0.41t_1$ as well as $\mu = 1.48t_0$.

The $4d_{xz}$ and $4d_{yz}$ orbitals form the so-called α and β sheets of the Fermi surface. They are characterized by a dispersion

$$h = \begin{pmatrix} \varepsilon_{xz} & V \\ V & \varepsilon_{yz} \end{pmatrix} \tag{B3}$$

with

$$\begin{aligned} \varepsilon_{\boldsymbol{k},xz} &= \varepsilon_x^{(0)} - 2t_{2,x}\cos k_x - 2t_{3,y}\cos k_y - \mu, \\ \varepsilon_{\boldsymbol{k},yz} &= \varepsilon_y^{(0)} - 2t_{2,y}\cos k_y - 2t_{3,x}\cos k_x - \mu, \\ V_{\boldsymbol{k}} &= -2t_{5,+}\cos(k_x+k_y) + 2t_{5,-}\cos(k_x-k_y) \end{aligned} \tag{B4}$$

with $t_{2,3,i} = t_{2,3}(1-\beta\epsilon_{ii})$ and $t_{5,\pm}/t_5 = 1-\frac{\beta}{2}(\epsilon_{xx}+\epsilon_{yy}\pm 2\epsilon_{xy})$. For the hopping elements of the unstrained system we use the values given in Ref. [11]: $t_2 = 0.165\,\mathrm{eV}$, $t_3 = 0.08t_2$, and $t_5 = 0.13t_2$. Finally, for the unstrained system holds $\varepsilon_x^{(0)} - \mu = \varepsilon_y^{(0)} - \mu = -0.18t_2$.

APPENDIX C: THE KINEMATIC GAP IN THE SINGLE-BAND MODEL

We can parametrize the momenta $\mathbf{k} = (k_x, k_y)$ of the γ band according to

$$k_x = \pm f(k_y) = \pm \arccos\left(-\frac{t_{1,y}\cos k_y + \mu}{t_{1,x} + 2t_{4,\pm}\cos k_y}\right). \tag{C1}$$

It holds that $\mathbf{k}_{1,y} = -\mathbf{k}_{3,y}$ for the smallest possible momentum transfer between Fermi surfaces of two neighboring Brillouin zones. Using that momentum is conserved in each component up to a reciprocal lattice vector, the momentum closest to the Van Hove point that can still participate in a $cc \leftrightarrow ch$ scattering process is determined by

$$2f\left(\frac{\pi - \mathbf{k}_{2,y}}{2}\right) + f(\mathbf{k}_{2,y}) = 2\pi, \tag{C2}$$

yielding $\mathbf{k}_{2,x} = 0.887\pi$. Every point closer to the Van Hove point can not participate in $cc \leftrightarrow ch$ scattering events since the momentum transfer is not big enough to induce umklapp scattering.

APPENDIX D: SINGLE-PARTICLE SELF-ENERGY

In this Appendix we analyze the single-particle self-energy of Eq. (37) that describes the scattering of electrons with momentum $\boldsymbol{k}_1$ with density fluctuations described by Eqs. (11)–(13). We consider the imaginary part of the self-energy as given in Eq. (15).

We want to analyze a generic point on the Fermi surface, away from the Van Hove singularity. Given the small momentum transfer we assume that $\boldsymbol{k}$ and $\boldsymbol{k}'$ are points nearby on the Fermi surface of similar length k_F. Thus, we can safely assume a constant density of states ρ_F for these states. As follows from Eq. (12), the momentum dependence of the density fluctuation spectrum is determined solely by $\varepsilon_{\mathrm{VH},\boldsymbol{k}-\boldsymbol{k}'}$ with saddle point dispersion $\varepsilon_{\mathrm{VH},\boldsymbol{k}}$ of Eq. (10). If we use $\boldsymbol{k} = k_F(\cos\theta, \sin\theta)$ and $\boldsymbol{k}' = k_F(\cos\phi, \sin\phi)$, we obtain for small $\varphi = \theta - \phi$ that

$$\varepsilon_{\mathrm{VH},\boldsymbol{k}-\boldsymbol{k}'} \approx -\varepsilon_{\mathrm{VH},\boldsymbol{k}}\varphi^2 + \frac{k_x k_y}{4m}\varphi^3. \tag{D1}$$

We first analyze the self-energy at $T=0$ as function of frequency. Considering without restriction $\omega > 0$ the condition coming from the Fermi and Bose functions is that $0 <$

$\epsilon_c(\boldsymbol{p}) < \omega$. This yields

$$\mathrm{Im}\Sigma(\boldsymbol{k},\omega) = 2U^2\rho_F \int_0^{\omega} d\varepsilon_c \int_0^{2\pi} d\varphi \mathrm{Im}\Pi(\boldsymbol{k}-\boldsymbol{p},\varepsilon_c). \tag{D2}$$

Let us first consider momenta $\boldsymbol{k}$ with $\varepsilon_{\mathrm{VH},\boldsymbol{k}} \neq 0$, i.e., $\theta \neq (2l+1)\frac{\pi}{4}$. With $s \equiv |\varepsilon_{\mathrm{VH},\boldsymbol{k}}|\varphi^2 \approx D\varphi^2$ follows

$$\begin{aligned}\mathrm{Im}\Sigma(\boldsymbol{k},\omega) &= -\frac{U^2\rho_F}{\sqrt{D}} \int_0^{\omega} d\epsilon \int_0^{\infty} \frac{ds}{\sqrt{s}} \mathrm{Im}\Pi(\boldsymbol{k}-\boldsymbol{p},\epsilon) \\ &= -\frac{U^2\rho_F}{\sqrt{D}} \int_0^{\omega} d\epsilon \left(\int_{\epsilon}^{\infty} \frac{ds\epsilon}{s^{3/2}} + \int_0^{\epsilon} \frac{ds}{s^{1/2}} \right) \\ &= -\frac{8U^2\rho_F^2}{3\sqrt{D}} |\omega|^{3/2}. \end{aligned} \tag{D3}$$

For the special momenta with $\theta = (2l+1)\frac{\pi}{4}$, where $\varepsilon_{\mathrm{VH},\boldsymbol{k}} = 0$ one should use $s \propto \varphi^3$ and it follows $\mathrm{Im}\Sigma(\boldsymbol{k},\omega) \propto |\omega|^{4/3}$. Those results were earlier obtained in Ref. [27]. If, instead, the dispersion $\varepsilon_c(\boldsymbol{k})$ is assumed to be equal to $\varepsilon_{\mathrm{VH},\boldsymbol{k}}$ one finds $\mathrm{Im}\Sigma(\boldsymbol{k},\omega) \propto |\omega|$. This result was obtained in Ref. [28].

At finite temperatures the analysis proceeds in an analogous manner and one obtains

$$\mathrm{Im}\Sigma(\boldsymbol{k},\varepsilon_{\boldsymbol{k}}) \approx -\frac{8U^2\rho_F^2}{3\sqrt{D}} (T)^{3/2} \tag{D4}$$

for generic momenta and corresponding results for special directions. This result is crucial for the thermal transport behavior.

APPENDIX E: CHARGE TRANSPORT RATE WITHIN THE MEMORY FUNCTION FORMALISM

The optical conductivity $\mathbf{j}(\omega) = \sigma(\omega)\mathbf{E}(\omega)$ obtained by the Kubo formula is

$$\sigma_{\alpha\beta}(\omega) = \frac{i}{\omega}(\langle T_{\alpha\beta}\rangle + \chi_{j_\alpha j_\beta}(\omega)) \tag{E1}$$

with inverse mass tensor $T_{\alpha\beta} = \frac{e^2}{N}\sum_{\mathbf{k}\sigma} \frac{\partial^2\varepsilon(\mathbf{k})}{\partial k_\alpha \partial k_\beta} c^\dagger_{k\sigma} c_{k\sigma}$ and current-current susceptibility $\chi_{j_\alpha j_\beta}$. If the current is conserved this reduces to $\sigma_{\alpha\beta}(\omega) = \frac{i\langle T_{\alpha\beta}\rangle}{\omega}$. Then the real part of the conductivity diverges as ω approaches zero, making it impossible to include a current-relaxing interaction by perturbation theory in the low-frequency limit. This problem can be tackled by introducing the memory matrix [37] $M_{\alpha\beta}$ as a correction to the ω^{-1}-behavior and regain the low-frequency expansion of the conductivity

$$\sigma_{\alpha\beta}(\omega) = \frac{i\langle T_{\alpha\beta}\rangle}{\omega + M_{\alpha\beta}(\omega)}. \tag{E2}$$

The imaginary part of the memory function determines the scattering rate $\tau_J^{-1}(\omega)$. The memory function contains the current-relaxing processes and can more easily be treated within perturbation theory. By comparing with Eq. (E1) we find that the memory function up to first order in the interaction is

$$M_{\alpha\beta}(\omega) \approx \frac{\omega\chi_{j_\alpha j_\beta}(\omega)}{\langle T_{\alpha\beta}\rangle}. \tag{E3}$$

This expansion is valid for $\omega \gg \tau_J^{-1}(0)$. We can rewrite this as

$$M_{\alpha\beta}(\omega) \approx \frac{\langle [F_\alpha F_\beta]\rangle - \chi_{F_\alpha F_\beta}(\omega)}{\omega\langle T_{\alpha\beta}\rangle}, \tag{E4}$$

where $F_\alpha = [j_\alpha, H]$ follows from the equation of motion for $\chi_{j_\alpha j_\beta}(\omega)$. The scattering rate is therefore given by

$$\tau_J^{-1}(\omega) = \frac{-\mathrm{Im}\chi_{F_\alpha F_\beta}(\omega)}{\omega\langle T_{\alpha\beta}\rangle} \tag{E5}$$

with

$$\begin{aligned}\chi_{F_\alpha F_\beta}(\omega) = e^2U^2 &\sum_{\mathbf{k}_1\ldots\mathbf{k}_4} (v_{k_1} + v_{k_2} - v_{k_3} - v_{k_4})^2 \\ &\times L_{\varepsilon_{\mathbf{k}_1}\varepsilon_{\mathbf{k}_2}\varepsilon_{\mathbf{k}_3}\varepsilon_{\mathbf{k}_4}} \sum_{\mathbf{G}} \delta_{\mathbf{k}_1+\mathbf{k}_2-\mathbf{k}_3-\mathbf{k}_4-\mathbf{G}} \\ &\times \left[\frac{1}{\omega + \varepsilon_{\mathbf{k}_1} + \varepsilon_{\mathbf{k}_2} - \varepsilon_{\mathbf{k}_3} - \varepsilon_{\mathbf{k}_4}} \right. \\ &\left. - \frac{1}{\omega - \varepsilon_{\mathbf{k}_1} - \varepsilon_{\mathbf{k}_2} + \varepsilon_{\mathbf{k}_3} + \varepsilon_{\mathbf{k}_4}} \right]. \end{aligned} \tag{E6}$$

The imaginary part of the susceptibility can be evaluated in analogy to $\tau_J(0)$, where the external frequency replaces temperature. Taking into account the proper phase space for umklapp scattering, this yields a frequency depending scattering rate

$$\tau_J^{-1}(\omega) = \lambda_0 \frac{\omega^2}{D} \log\left(\frac{D}{|\omega|}\right). \tag{E7}$$

This result, valid in the regime $\tau_J^{-1}(\omega = 0) \ll \omega \ll D$, gives rise to the optical conductivity given in Eq. (28). The rate is therefore determined by the same processes that give rise to the temperature dependence of the resistivity. As was discussed in Refs. [38,39] for higher frequencies, shorter rates that do not rely on the condition of momentum conservation may also affect the frequency dependence of the optical conductivity. Here, the shorter single-particle rate $\sim\omega^{3/2}$ could become relevant. For our problem those would only become relevant once ω becomes comparable to the band width D. Thus is unclear whether such an intermediate regime will be observable in experiment. At lowest frequencies the result Eq. (E7) is however the dominant one.

[1] A. P. Mackenzie and Y. Maeno, The superconductivity of Sr_2RuO_4 and the physics of spin-triplet pairing, Rev. Mod. Phys. **75**, 657 (2003).

[2] A. P. Mackenzie, T. Scaffidi, C. W. Hicks, and Y. Maeno, Even odder after twenty-three years: The superconducting order parameter puzzle of Sr_2RuO_4, npj Quantum Mater. **2**, 40 (2017).

[3] C. W. Hicks, D. O. Brodsky, E. A. Yelland, A. S. Gibbs, J. A. N. Bruin, M. E. Barber, S. D. Edkins, K. Nishimura, S. Yonezawa, Y. Maeno, and A. P. Mackenzie, Strong increase of T_c of Sr_2RuO_4 under both tensile and compressive strain, Science **344**, 283 (2014).

[4] V. Grinenko, S. Ghosh, R. Sarkar, J.-C. Orain, A. Nikitin, M. Elender, D. Das, Z. Guguchia, F. Brückner, M. E. Barber *et al.*, Split superconducting and time-reversal symmetry-breaking transitions, and magnetic order in Sr_2RuO_4 under uniaxial stress, Nat. Phys. **17**, 748 (2021).

[5] Y.-S. Li, M. Garst, J. Schmalian, N. Kikugawa, D. A. Sokolov, C. W. Hicks, F. Jerzembeck, M. S. Ikeda, A. W. Rost, M. Nicklas, and A. P. Mackenzie, Elastocaloric determination of the phase diagram of Sr_2RuO_4, arXiv:2201.04147.

[6] Y.-S. Li, N. Kikugawa, D. A. Sokolov, F. Jerzembeck, A. S. Gibbs, Y. Maeno, C. W. Hicks, J. Schmalian, M. Nicklas, and A. P. Mackenzie, High sensitivity heat capacity measurements on Sr_2RuO_4 under uniaxial pressure, Proc. Natl. Acad. Sci. USA **118**, e2020492118 (2021).

[7] I. M. Lifshitz, Anomalies of electron characteristics of a metal in the high pressure region, Zh. Eksp. Teor. Fiz. **38**, 1569 (1960) [Sov. Phys. JETP **11**, 1130 (1960)].

[8] M. E. Barber, A. S. Gibbs, Y. Maeno, A. P. Mackenzie, and C. W. Hicks, Resistivity in the Vicinity of a Van Hove Singularity: Sr_2RuO_4 under Uniaxial Pressure, Phys. Rev. Lett. **120**, 076602 (2018).

[9] N. Kikugawa, C. Bergemann, A. P. Mackenzie, and Y. Maeno, Band-selective modification of the magnetic fluctuations in Sr_2RuO_4: A study of substitution effects, Phys. Rev. B **70**, 134520 (2004).

[10] K. M. Shen, N. Kikugawa, C. Bergemann, L. Balicas, F. Baumberger, W. Meevasana, N. J. C. Ingle, Y. Maeno, Z.-X. Shen, and A. P. Mackenzie, Evolution of the Fermi Surface and Quasiparticle Renormalization through a Van Hove Singularity in $Sr_{2-y}La_yRuO_4$, Phys. Rev. Lett. **99**, 187001 (2007).

[11] B. Burganov, C. Adamo, A. Mulder, M. Uchida, P. D. C. King, J. W. Harter, D. E. Shai, A. S. Gibbs, A. P. Mackenzie, R. Uecker, M. Bruetzam, M. R. Beasley, C. J. Fennie, D. G. Schlom, and K. M. Shen, Strain Control of Fermiology and Many-Body Interactions in Two-Dimensional Ruthenates, Phys. Rev. Lett. **116**, 197003 (2016).

[12] R. Franz and G. Wiedemann, Ueber die Wärme-Leitungsfähigkeit der Metalle, Ann. Phys. **165**, 497 (1853).

[13] R. Hlubina and T. M. Rice, Resistivity as a function of temperature for models with hot spots on the Fermi surface, Phys. Rev. B **51**, 9253 (1995); **52**, 13043(E) (1995).

[14] R. Hlubina, Effect of impurities on the transport properties in the Van Hove scenario, Phys. Rev. B **53**, 11344 (1996).

[15] F. Herman, J. Buhmann, M. H. Fischer, and M. Sigrist, Deviation from Fermi-liquid transport behavior in the vicinity of a Van Hove singularity, Phys. Rev. B **99**, 184107 (2019).

[16] B. P. Stojkovic and D. Pines, Anomalous Hall Effect in $YBa_2Cu_3O_7$, Phys. Rev. Lett. **76**, 811 (1996).

[17] A. Rosch, Interplay of Disorder and Spin Fluctuations in the Resistivity near a Quantum Critical Point, Phys. Rev. Lett. **82**, 4280 (1999).

[18] S. V. Syzranov and J. Schmalian, Conductivity Close to Antiferromagnetic Criticality, Phys. Rev. Lett. **109**, 156403 (2012).

[19] C. H. Mousatov, E. Berg, and S. A. Hartnoll, Theory of the strange metal $Sr_3Ru_2O_7$, Proc. Natl. Acad. Sci. USA **117**, 2852 (2020).

[20] J. M. Ziman, *Electrons and Phonons* (Oxford University Press, Oxford, 1960).

[21] C. Castellani, C. DiCastro, G. Kotliar, P. A. Lee, and G. Strinati, Thermal Conductivity in Disordered Interacting-Electron Systems, Phys. Rev. Lett. **59**, 477 (1987).

[22] K. Michaeli and A. M. Finkelstein, Quantum kinetic approach for studying thermal transport in the presence of electron-electron interactions and disorder, Phys. Rev. B **80**, 115111 (2009).

[23] H. K. Pal, V. I. Yudson, and D. L. Maslov, Resistivity of non-Galilean-invariant Fermi- and non-Fermi liquids, Lith. J. Phys. **52**, 142 (2012)

[24] A. O. Lyakhov and E. G. Mishchenko, Thermal conductivity of a two-dimensional electron gas with Coulomb interaction, Phys. Rev. B **67**, 041304(R) (2003).

[25] M. W. Haverkort, I. S. Elfimov, L. H. Tjeng, G. A. Sawatzky, and A. Damascelli, Strong Spin-Orbit Coupling Effects on the Fermi Surface of Sr_2RuO_4 and Sr_2RhO_4, Phys. Rev. Lett. **101**, 026406 (2008).

[26] H. S. Røising, T. Scaffidi, F. Flicker, G. F. Lange, and S. H. Simon, Superconducting order of Sr_2RuO_4 from a three-dimensional microscopic model, Phys. Rev. Research **1**, 033108 (2019).

[27] S. Gopalan, O. Gunnarson, and O. K. Andersen, Effects of saddle-point singularities on the electron lifetime, Phys. Rev. B **46**, 11798 (1992).

[28] P. C. Pattnaik, C. L. Kane, D. M. Newns, and C. C. Tsuei, Evidence for the Van Hove scenario in high-temperature superconductivity from quasiparticle-lifetime broadening, Phys. Rev. B **45**, 5714 (1992).

[29] A. Matthiessen and C. Vogt, Ueber den Einfluss der Temperatur auf die elektrische Leitungsfähigkeit der Legierungen, Ann. Phys. Chem. **198**, 19 (1864); On the influence of temperature on the electric conducting-power of alloys, Philos. Trans. R. Soc. London **154**, 167 (1864).

[30] W. E. Lawrence and J. W. Wilkins, Electron-electron scattering in the transport coefficients of simple metals, Phys. Rev. B **7**, 2317 (1973); **13**, 2717(E) (1976).

[31] W. W. Schulz and P. B. Allen, Transport in metals with electron-electron scattering, Phys. Rev. B **52**, 7994 (1995).

[32] R. Mahajan, M. Barkeshli, and S. A. Hartnoll, Non-Fermi liquids and the Wiedemann-Franz law, Phys. Rev. B **88**, 125107 (2013).

[33] A. Principi and G. Vignale, Violation of the Wiedemann-Franz Law in Hydrodynamic Electron Liquids, Phys. Rev. Lett. **115**, 056603 (2015).

[34] S. A. Hartnoll, A. Lucas, and S. Sachdev, *Holographic quantum matter*, (MIT Press, Cambridge, MA, 2016).

[35] Strictly speaking, the thermal resistivity of a clean system is nonzero in the absence of umklapp scattering if it is measured under conditions of zero electrical current.

[36] J. Paglione, C. Lupien, W. A. MacFarlane, J. M. Perz, L. Taillefer, Z. Q. Mao, and Y. Maeno, Elastic tensor of Sr_2RuO_4, Phys. Rev. B **65**, 220506(R) (2002).

[37] W. Götze and P. Wölfle, Homogeneous dynamical conductivity of simple metals, Phys. Rev. B **6**, 1226 (1972).

[38] A. Rosch and N. Andrei, Conductivity of a Clean One-Dimensional Wire, Phys. Rev. Lett. **85**, 1092 (2000).

[39] A. Rosch and N. Andrei, Optical conductivity and pseudo-momentum conservation in anisotropic Fermi liquids, J. Low Temp. Phys. **126**, 1195 (2002).